Chapter 22

Effects of Axial Coordination, Electronic Excitation and Oxidation on Bond Orders in the Bacteriochlorin Macrocycle, and Generation of Radical Cation on Photo-Excitation of in vitro and in vivo Bacteriochlorophyll *a* Aggregates: Resonance Raman Studies

Yasushi Koyama*[1], Yoshinori Kakitani[1], Leenawaty Limantara[2] and Ritsuko Fujii[1]
[1] Faculty of Science and Technology, Kwansei Gakuin University, 2-1 Gakuen, Sanda, Hyogo 669-1337, Japan; [2] Faculty of Science and Mathematics, Satya Wacana Christian University, Jl. Diponegoro 52-60, Salatiga 50711, Indonesia

Note: Readers are encouraged to visit the website http://epub.ub.uni-muenchen.de/archive/00000776/ for 'supplementary material,' where Figs. S1–S7 referred to in the text are posted.

*Author for correspondence, email: ykoyama@kwansei.ac.jp

Bernhard Grimm, Robert J. Porra, Wolfhart Rüdiger and Hugo Scheer (eds): Chlorophylls and Bacteriochlorophylls: Biochemistry, Biophysics, Functions and Applications, pp. 323–335.

Summary

Solutions of bacteriochlorophyll (BChl) *a* in both monomeric and aggregated forms, and also in solutions of pigment-protein complexes, were examined by resonance-Raman spectroscopy. The results permit us to report and discuss:

(1) The effects of axial coordination forming the 5- and 6-coordinated states as well as those of triplet excitation and one-electron oxidation forming the T_1 (lowest triplet) and the D_0 (radical-cation) states on bond orders in the macrocycle of BChl *a*, as probed by the ring-breathing frequency. A core-expansion mechanism is proposed by which the ring-breathing frequency reflects the coordination states in the S_0, T_1 and D_0 electronic states. Solvent parameters determining the relative stabilities of the 5- and 6-coordinated states are also discussed.

(2) Changes in bond order in the macrocycles of BChl *a* and bacteriopheophytin *a* upon photo-excitation to the T_1 and S_1 (the first-excited singlet) states as determined by changes in stretching force constants that were obtained by normal-coordinate analysis of the Raman spectra of the unlabeled and totally ^{15}N-, ^{13}C- and ^{2}H-labeled species. Based on the results, the implications of the pigment arrangement in the reaction center, facilitating electron transfer and triplet energy-transfer reactions, are discussed in terms of the partial localization of the HOMO and LUMO (the highest occupied and the lowest unoccupied molecular orbitals) that were identified as large changes in bond order.

(3) The generation of the T_1 state and subsequent transformation into the D_0 state on photo-excitation of BChl *a* aggregates, both in solution and in the carotenoid-less light harvesting complexes, LH1 and LH2. These have been identified by the use of the key ring-breathing Raman lines in the T_1 and D_0 states, and then, confirmed by electronic-absorption and EPR spectroscopy.

I. The 5- and 6-Coordinated States of Bacteriochlorophyll *a* in the S_0, T_1 and D_0 Electronic States as Probed by the Ring-Breathing Frequency

A. The Ring-Breathing Frequencies in the S_0, T_1 and D_0 States

1. The S_0 State

The strongest Raman line of bacteriochlorophyll (BChl) *a* was associated with the C_a–C_m and $C_{a'}$–C_m stretchings (Lutz, 1984; Donohoe et al., 1988; Hu et al., 1993); see Fig. 1 for the designation of carbon atoms in the conjugated part of the macrocycle. The assignment has been established to be the C_a–C_m and $C_{a'}$–C_m asymmetric stretchings coupled with C_a–C_b stretchings (simplified as 'the C_a–C_m asymmetric stretching') based on the normal-coordinate analysis of unlabeled and isotope-labeled BChl *a* (Sashima et al., 2000) as will be described in Sec. II A. Since this normal mode causes the shrinkage and expansion of the inner 16-membered ring of the BChl *a* macrocycle, we name it 'the ring-breathing mode.' In particular, we will call the ring-breathing mode in the S_0 state as 'ν_r'. By the use of the ν_r frequency, Callahan and Cotton (1987) classified the axial coordination of BChl *a* into the 5- and 6-coordinated states after measuring the ν_r Raman line in 15 different solvents and concluded that it appears at 1609 cm^{-1} and at 1595 cm^{-1} in the 5- and 6-coordinated states, respectively. Table 1 lists the ν_r frequencies in 20 different solvents; those solvents giving rise to a mixture of the 5- and 6-coordinated states are excluded (Y. Umemoto, K. Furukawa and Y. Koyama, unpublished; Nishizawa et al., 1994a; Misono et al., 1996; Koyama and Limantara, 1998). Actually, the ν_r frequency is in the region of 1605–1611 cm^{-1} in the 5-coordinated state and between 1594–1599 cm^{-1} in the 6-coordinated state.

The basis for the classification into the 5- and 6-coordinated states is as follows: When BChl *a* was dissolved in highly electron-donating (i.e., strongly-ligating) solvents such as methanol, pyridine

Abbreviations: BChl – bacteriochlorophyll; BPhe – bacteriopheophytin; Car – carotenoid; DN – donor number; D_0 – the radical-cation state; HOMO – highest occupied molecular orbital; LH1, LH2 – light harvesting complexes 1 and 2; LUMO – lowest unoccupied molecular orbital; MO – molecular orbital; *Rba. – Rhodobacter*; RC – reaction center; S_0 – the ground state; S_1 – the first singlet-excited state; T_1 – the lowest triplet-excited state; ν_r – the ring-breathing frequency in the S_0 state; ν_r' – the ring-breathing frequency in the S_1 state; ν_r'' – the ring-breathing frequency in the T_1 state; ν_r^+ – the ring-breathing frequency in the D_0 state

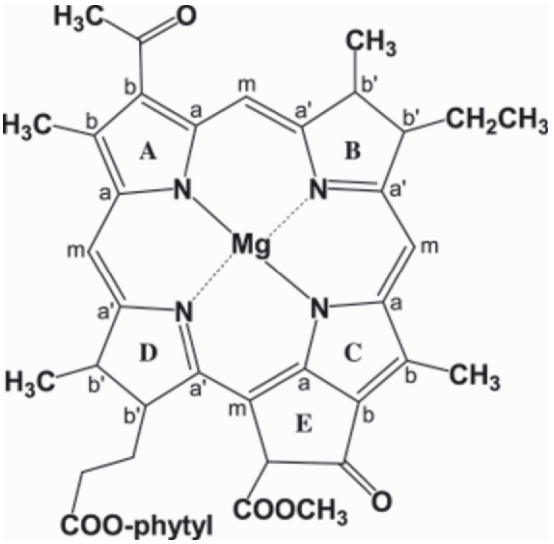

Fig. 1. Chemical structure of BChl *a* and designation of the rings and the carbon atoms in the macrocycles.

and tetrahydrofuran, the ν_r Raman line appeared at 1596, 1594 and 1595 cm^{-1}, respectively. When those solvents were diluted with methylene chloride, the ν_r Raman line shifted to 1609 cm^{-1}. The above changes in the ν_r frequency were ascribed to transformation from the 6- to the 5-coordinated state, respectively (Callahan and Cotton, 1987). In general, those solvents having high and low electron-donating power tend to form the 6- and 5-coordinated states, respectively (see Sec. B for the detailed mechanism).

2. The T_1 State

Nishizawa et al. (1994a) recorded the T_1 Raman spectra of BChl *a* in 16 different solvents (the raw Raman data are presented in Fig. S1; hereafter, figures appearing in supplementary material will be numbered as S2, S3, ...). Table 1 also lists the frequencies of the ring-breathing mode in the T_1 state (hereafter called 'ν_r'''). The ν_r'' frequencies are in the 1585–1591 cm^{-1} or in the 1578–1581 cm^{-1} regions in solvents having low and high electron-donating power, respectively. Therefore, it is reasonable to conclude that T_1 BChl *a* is in the 5- (6-) coordinated state in the former (the latter) solvents. Table 1 lists the resultant classification into the pair of coordinating states in the T_1 state, which is in complete agreement with that in the S_0 state. The ν_r'' frequencies in general are much lower than the ν_r frequencies, but both of them are definitely lower in the 6-coordinated state than in the 5-coordinated state.

3. The D_0 State

Misono et al. (1996) measured the Raman spectra of BChl *a* in the radical-cation (D_0) state that was generated electrochemically by one-electron oxidation in 13 different solvents (the raw Raman data are presented in Fig. S2). Hereafter, we *mainly* use the term 'the D_0 state' as an electronic state of BChl *a* and the term 'radical cation' in reference to the chemical species. Table 1 also lists the frequencies of the ring-breathing mode in the D_0 state (hereafter called 'ν_r^+'). The ν_r^+ frequencies are in the 1595–1599 cm^{-1} or in the 1584–1588 cm^{-1} regions in solvents having low and high electron-donating power, respectively; therefore, the former and latter regions can be ascribed to the 5- and 6-coordinated states, respectively. In general, the ν_r^+ frequencies are between the ν_r and ν_r'' frequencies, and the ν_r^+ frequencies in the 6-coordinated state are lower than those in the 5-coordinated state. Here again, the two coordination states exhibit two distinct frequency regions. (The ν_r, ν_r'' and ν_r^+ frequency regions in general and in the 5- and 6-coordinated states are summarized in Table S1.)

B. Mechanisms by Which the Ring-Breathing Frequency Reflects the 5- and 6-Coordinated States

Two possible mechanisms by which the ring-breathing frequency reflects the 5- and 6-coordinated states have been proposed, i.e., the core-expansion mechanism and the axial-polarization mechanism (Nishizawa et al., 1994a). The mechanisms were originally proposed for the T_1 state of BChl *a*; however, they should apply to the S_0 and the D_0 states as well.

1. The Core-Expansion Mechanism

When the central Mg atom of BChl *a* has only one axial ligand (in addition to the four nitrogen atoms in the macrocycle; see Fig. 1), it can sit out of the macrocycle plane. When the Mg atom has two equivalent axial ligands, however, it needs to sit in the macrocycle plane, and then, the 16-membered ring is to be expanded. Therefore, the lower ring-breathing frequency in the 6-coordinated state is supposed to reflect decrease in bond order in the expanded 16-membered ring (alternatively called 'the core').

2. The Axial-Polarization Mechanism

When the oxygen or nitrogen atom of the solvent

Table 1. The ring-breathing frequencies in the S_0 (ν_r), T_1 (ν_r'') and D_0 (ν_r^+) states of BChl *a* for classification into the 5-coordinated (V) and the 6-coordinated (VI) states, and those in the S_1 (ν_r') state. Solvent parameters to determine the relative stability of the two coordination states, in solution and bound to pigment-protein complexes (see foot notes), are also listed.

solvents / complexes	the ring-breathing frequencies										solvent parameters		
	ν_r		ν_r''		ν_r^+		ν_r'		$\nu_r^{+\,a}$		DN [b]	β [c]	π^* [d]
acetonitrile	1606	V	1590	V							14.1	0.31	0.75
propionitrile	1611	V			1597	V					16.1	0.37	0.71
1-butyronitrile	1609	V			1596	V					16.6		0.71
acetone	1608	V	1588	V	1598	V	1568				17.0	0.48	0.71
2-butanone	1610	V	1586	V	1595	V						0.48	0.67
3-pentanone	1610	V	1590	V	1596	V						0.45	0.72
2-octanone	1608	V	1589	V	1599	V							
diethyl ether	1607	V	1591	V							19.2	0.47	0.27
propyl ether	1608	V	1591	V									
methylene chloride	1609	V			1599	V			1597	V		0.00	0.82
carbon tetrachloride	1605	V							1599	V		0.00	0.28
2-propanol	1608	V	1585	V	1588	VI						0.95	0.48
methanol	1596	VI			1584	VI					19.0	0.62	0.60
ethanol	1599	VI			1585	VI					20.0	0.77	0.54
1-propanol	1598	VI			1584	VI							0.52
1-butanol	1597	VI	1580	VI	1588	VI						0.88	0.47
1-hexanol	1594	VI	1578	VI									
1-decanol	1596	VI	1579	VI									
pyridine	1594	VI	1581	VI			1568				33.1	0.64	0.87
tetrahydrofuran	1595	VI	1580	VI	1586	VI	1567				20.0	0.55	0.58
LH1	1610	V	1590	V					1596	V			
LH2	1608	V	1589	V					1596	V			
RC	1609	V							1598, 1599	V			

[a] Radical cation generated by photo-excitation. [b] Donor number which scale the electron-donating power of the solvent (Gutmann, 1978). [c] Taft parameter scaling the electron-donating power of the solvent (Kamlet et al., 1983). [d] Taft parameter scaling dielectric stabilization of a dipole by the solvent system (Kamlet et al., 1977, 1983; Kamlet and Taft, 1979)

molecule axially ligates the magnesium atom in the bacteriochlorin macrocycle, some electronic charge is to be transferred from the ligand to the metal. A Pariser-Parr-Pople calculation (Nishizawa et al., 1994a) including configurational interactions predicts that this axial polarization, (i.e., an effective positive charge on the oxygen or nitrogen atom and a negative charge on the magnesium atom) which should cause decrease in the bond orders of the $C_{a'}$–C_m, C_a–C_m and C_a–C_b bonds leading to decreased ring-breathing frequency and increased bond orders of the C_a–N, C_b–C_b and $C_{a'}$–N bonds (see Fig. 1 for the designation of the carbon atoms). Such changes upon ligation can take place in both coordination states; the calculated effects should be doubled in the 6-coordinated state with two axial ligands.

The core-expansion mechanism neatly explains the large and discrete change in the ring-breathing frequency upon transformation from the 5- to the 6-coordinated state in each electronic state. Comparison of the ring-breathing frequencies between BChl *a* and bacteriopheophytin (BPhe) *a* in the S_0, T_1 and S_1 states (see Table S1) rationalizes the core-expansion mechanism: in both the S_0 and the T_1 states, the ring-breathing frequencies of BChl *a* in the 5-coordinated state (ν_r 1605–1611 cm^{-1} and ν_r'' 1585–1591 cm^{-1}) roughly agree with those of BPhe *a* (ν_r 1606–1610 cm^{-1} and ν_r'' 1586–1589 cm^{-1}). In both electronic states, those frequencies may reflect that the intrinsic bond order in the 16-membered ring are common to both BChl *a* and BPhe *a*. (In other words, because the magnesium atom is located out of the macrocycle plane in the 5-coordinated BChl *a*, the ring-breathing frequencies would not be affected by its presence.) In the 6-coordinated state of BChl *a*, however, the expansion of the 16-membered ring by the magnesium atom should cause the down-shift of the ring-breathing frequency as described in the previous section.

The frequencies of the ring-breathing mode in the S_1 state (called 'ν_r'') are much lower in BChl *a* (1567–1568 cm^{-1}) than in BPhe *a* (1582–1587 cm^{-1}) thus indicating that the electronic structure of BChl *a* differs from BPhe *a*, and that the bond orders in the 16-membered ring are substantially lower in BChl *a* than in BPhe *a*. Therefore, the ring may be so expanded in the S_1 state of BChl *a* that the presence of the magnesium atom in or out of the macrocycle plane may make no difference at all. (The ν_r, ν_r'' and ν_r' frequency regions of BPhe *a* are summarized and compared with those of BChl *a* in Table S1.)

C. Solvent Parameters Determining the Relative Stability of the 5- and 6-Coordinated States

The core-expansion mechanism predicts that the selection of one of the coordination states is due to a balance between the steric hindrance and the power of ligation: the steric hindrance between the magnesium atom and the core (the 16-membered ring) of the macrocycle must push the equilibrium toward the 5-coordinated state, whereas the stabilization on ligation of the solvent molecule must push it toward the 6-coordinated state. Therefore, solvent molecules having high or low electron-donating power are expected to form the 6- or 5-coordinated states, respectively. On the other hand, a strong axial dipole can be generated by ligation of a single solvent molecule in the 5-coordinated state, whereas a pair of dipoles formed by ligation of two equivalent solvent molecules should be canceled out in the 6-coordinated state. Therefore, the dielectric stabilization of the axial dipole can be an additional factor to determine the relative stability of the coordination states; strong (weak) dielectric stabilization is expected to shift the equilibrium toward the 5- (6-) coordinated state.

Table 1 shows that the classification into the two coordination states is consistent among all the S_0, T_1 and D_0 electronic states except for the case of 2-propanol, which will be discussed later. Table 1 also lists the relevant solvent parameters, such as DN (Gutmann, 1978), and Taft's β and π^* parameters (Kamlet et al., 1977, 1983; Kamlet and Taft, 1979), which supposedly determine the relative stability of the 5- and 6-coordinated states. The DN value indicates the electron-donating power of the solvent and, in general, those solvents having small (large) DN values tend to form the 5- (6-) coordinated state; an exception is diethyl ether that may cause strong ligating power but more serious steric hindrance. One of the Taft parameters, β, also measures the electron-donating power of the solvent. Figures 2a, b and c show the ν_r, ν_r'' and ν_r^+ frequencies as a function of β. Interestingly, the 5- (6-) coordinated state is formed whenever $\beta < 0.5$ ($\beta > 0.5$) in all the S_0, T_1 and D_0 electronic states. The other Taft parameter, π^*, indicates the dielectric stabilization of a dipole by the solvent system. Figure 2d shows that the 5- (6-) coordinated state is stabilized in those solvents having large (small) π^* values.

In the case of 2-propanol (see Table 1 and the shadowed plot in Fig. 2), the very high value of β

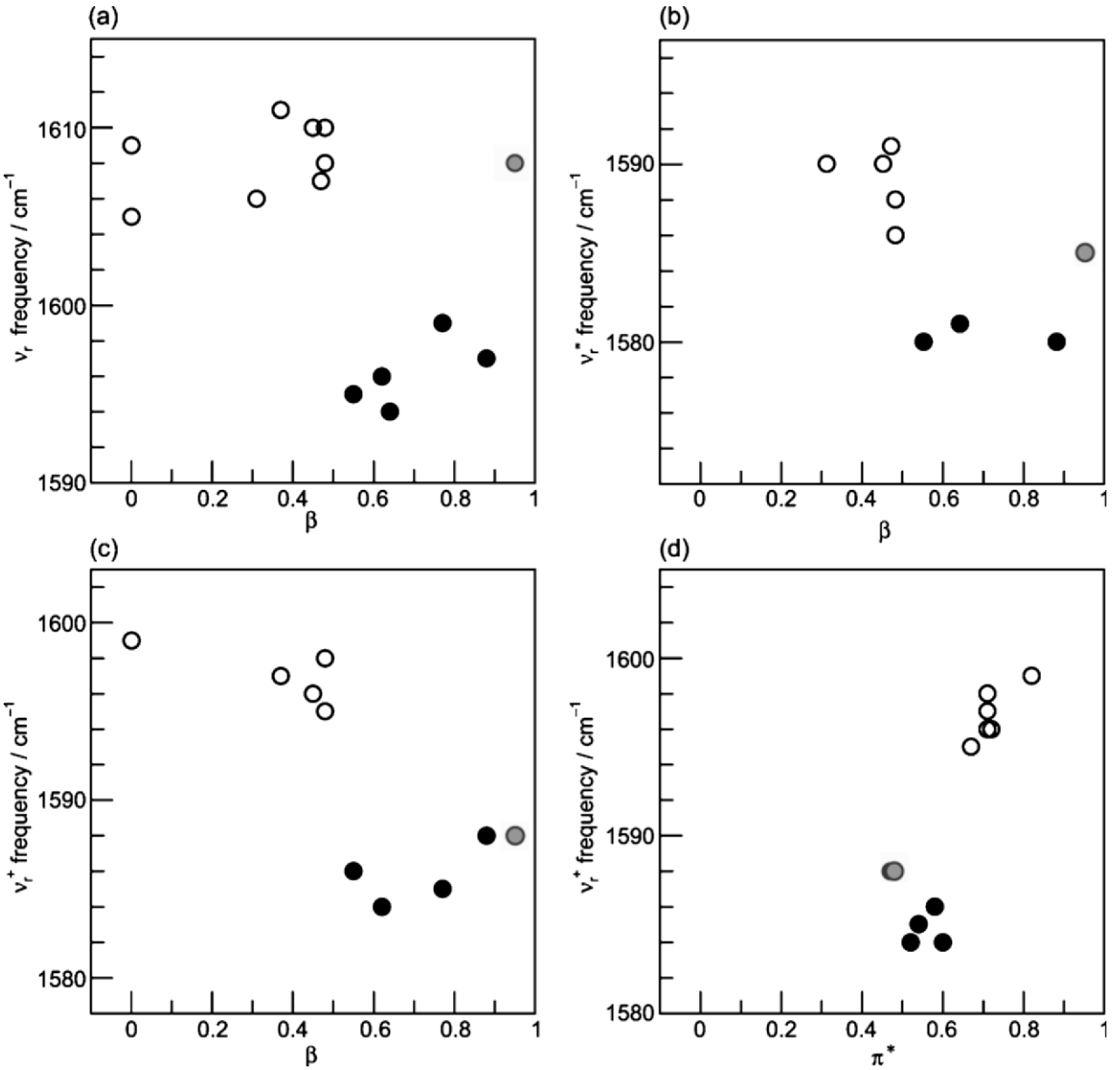

Fig. 2. Correlation between the ring-breathing frequencies reflecting the coordination states and the Taft parameters, β and π^* (Kamlet et al., 1977, 1983; Kamlet and Taft, 1979); β measures the electron-donating power of the solvent, whereas π^* indicates the dielectric stabilization of the dipole that is generated by ligation of the solvent. The (a) ν_r – β, (b) ν_r'' – β and (c) ν_r^+ – β correlations, and (d) the ν_r^+ – π^* correlation all in the 5- (○) and 6- (●) coordinated states. An exceptional case of the solvent, 2-propanol, is also indicated (gray circle).

and the very low value of π^* predict that the 6-coordinated state should be favorable. Presumably, strong steric interaction due to the structure of this particular solvent is expected to prevent the formation of the 6-coordinated state in the neutral S_0 and T_1 states. However, in the case of positively-charged radical cation (the D_0 state), stabilization on ligation becomes a predominant factor to form the 6-coordinated state. Thus, transformation from the 5- to the 6-coordinated state should take place upon one-electron oxidation.

II. Changes in Bond Orders as Scaled by Stretching Force Constants in the Conjugated Systems of Bacteriochlorophyll *a*, Bacteriopheophytin *a* and Carotenoid: Implication of the Arrangement of Those Pigments in the Reaction Center

A. Determination of the Normal Modes and the Stretching Force Constants in the Macrocycles of BChl a and BPhe a

Sashima et al. (2000) measured the Raman spectra of unlabeled and ^{15}N, ^{13}C and ^{2}H totally-labeled BChl *a* and BPhe *a* in the S_0, T_1 and S_1 states, and performed normal-coordinate analyses to establish the assignment of the Raman lines and to determine the stretching force constants of the carbon-carbon and the carbon-nitrogen bonds in the macrocycles. (The detailed results of the normal-coordinate analyses are shown in Figs. S3, S4 and S5.)

Figure 3 depicts the normal modes of the ring-breathing vibrations of BChl *a* and BPhe *a* in the S_0, T_1 and S_1 states, which justify the usage of these particular modes in probing the effects of coordination and electronic excitation in the bacteriochlorin macrocycle as described in Sec. I. Those normal modes are very similar to one another among the three different electronic states, and even between BChl *a* and BPhe *a*. The normal modes can be referred to as the C_a–C_m and $C_{a'}$–C_m stretchings coupled with the C_a–C_b stretchings (simplified as 'the C_a–C_m asymmetric stretching'), as defined at the beginning of the previous section.

Figure 4 depicts changes in the stretching force constants in the macrocycles of (a) BChl *a* and (b) BPhe *a* after singlet and triplet excitation (Sashima et al., 2000). The figure also includes changes in the stretching force constants on triplet excitation of the conjugated chain of a carotenoid (Car),15-*cis*-spheroidene, bound to the reaction center (RC) (Mukai-Kuroda et al., 2002). The changes in stretching force constants can be characterized as follows: *(a) BChl a.* On excitation to the S_1 state, the largest changes in the stretching force constants take place in the C_b–C_b bonds of ring A and ring C (+1.32), and the second largest changes take place in the $C_{a'}$–$C_{b'}$ bonds of ring B and ring D (+0.93). On excitation to the T_1 state, the largest changes take place in the $C_{a'}$–$C_{b'}$ bonds of rings B and D (+0.93), and the second largest changes in the C_a–N bonds (+0.40). *(b) BPhe a.* On excitation to the S_1 state, the largest changes in the stretching force constants take place in the C_b–C_b bonds of ring A and ring C (+1.36), and the second largest changes in the C_a–C_m and $C_{a'}$–C_m bonds of the 16-membered ring (–0.23). (Here, no changes take place at all in the $C_{a'}$–$C_{b'}$ bonds of rings B and D in contrast to the case of BChl *a*.) On excitation to the T_1 state, the largest changes take place in the $C_{a'}$–$C_{b'}$ bonds of rings B and D (+0.53), but the second largest changes take place in the C_a–N bonds (+0.28) and the C_b–C_b and C_a–C_b bonds of rings A and C (–0.28). *(c) Car.* On triplet excitation, the largest three changes in the stretching force constants take place in the C13=C14 (–0.73), C11=C12 (–0.59) and C12–C13 (+0.43) bonds.

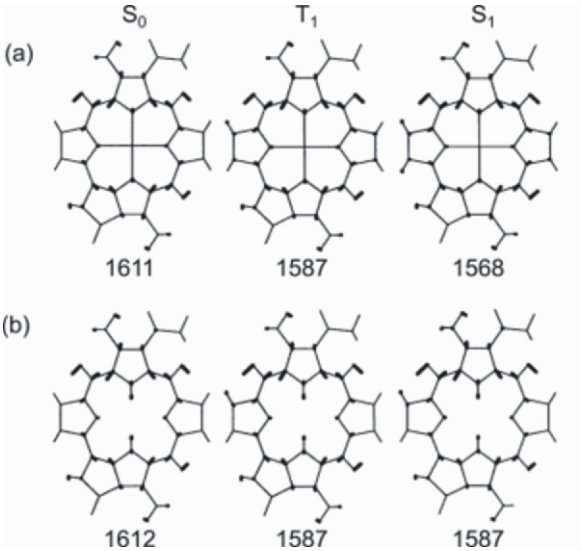

Fig. 3. Atomic displacements in the ring-breathing modes, i.e., 'the C_a–C_m asymmetric stretchings' in (a) BChl *a* and (b) BPhe *a* in the S_0, T_1 and S_1 states. The observed frequencies are also shown.

B. Localization of the Molecular Orbitals as Identified by Changes in Bond Orders upon Excitation, and the Arrangement of Pigment Molecules in the Reaction Center to Facilitate Charge Separation and Triplet Energy Transfer

In a Hückel-type molecular orbital (MO) description, where the MOs are expressed as a linear combination of the 2p atomic orbitals (χ_i) using coefficients (c_i) for atom *i*, the net change in bond order upon electronic excitation for an *a*–*b* bond is approximately given by $\Delta P_{ab} = -c_a^{\mathrm{HOMO}} \cdot c_b^{\mathrm{HOMO}} + c_a^{\mathrm{LUMO}} \cdot c_b^{\mathrm{LUMO}}$, where one of the coefficients, c_a or c_b, changes in its sign upon

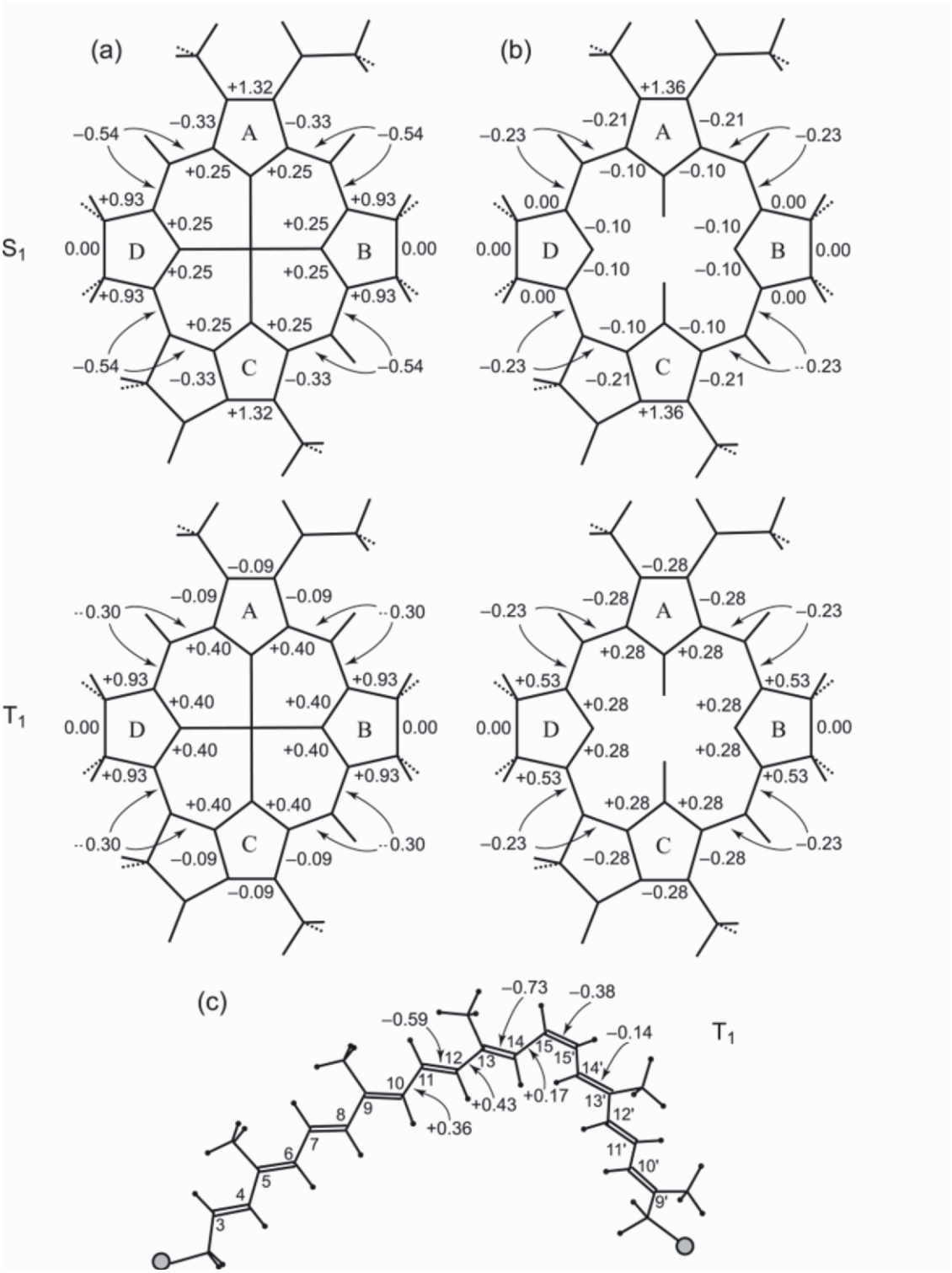

Fig. 4. Changes in the carbon-carbon and the carbon-nitrogen stretching force constants, upon singlet and triplet excitation, in the macrocycles of (a) BChl *a* and (b) BPhe *a* in solution, and (c) changes in the carbon-carbon stretching force constants, upon triplet excitation, in the conjugated chain of 15-*cis*-spheroidene bound to the RC.

the HOMO → LUMO transition. Here, partial localization of the HOMO and the LUMO in the macrocycle of BChl *a* (or BPhe *a*) is assumed. Then, a relation of $|\Delta P_{ab}| = |c_a^{\mathrm{HOMO}}| \cdot |c_b^{\mathrm{HOMO}}| + |c_a^{\mathrm{LUMO}}| \cdot |c_b^{\mathrm{LUMO}}|$ holds; ΔP_{ab} can be either positive or negative. When there is a large increase or decrease in bond order for the *a*–*b* bond, the absolute values of those coefficients will be large. Then, the HOMO (LUMO) of a molecule must be expanded spatially to facilitate their overlap with that of the neighboring molecule. Therefore, we can postulate that the charge-separation and the electron-transfer reactions, both using the overlap of the LUMOs of a pair of neighboring molecules, should be facilitated in a particular region where large changes in bond order upon singlet excitation take place in both the donor and the acceptor molecules. We can also postulate that the triplet energy-transfer reaction, using the overlap of both the HOMOs and LUMOs of the neighboring molecules, should be facilitated in a particular region where large changes in bond order take place upon triplet excitation in the donor and the acceptor molecules.

Figure 5 (and Color Plate 2) shows the arrangement of the BChl *a*, BPhe *a* and Car molecules in the RC from *Rhodobacter* (*Rba.*) *sphaeroides* strain AM260W that was determined by X-ray crystallography (R. J. Cogdell, personal communication). Now, changes in the stretching force constant, mentioned in the previous section, will be used as a scale for changes in bond order. In Fig. 5, in which the phytyl sidechains are truncated, bonds in the macrocycle giving rise to the largest and the second-largest changes in bond order (Fig. 4) are indicated by wavy and dotted lines, respectively. Based on the above postulates, we will explain the implications of the arrangement of those pigments from the viewpoint of the efficient charge-separation, electron-transfer and triplet energy-transfer reactions.

Charge Separation in the Special-Pair BChls. Figure 5a shows that a pair of C_b–C_b bonds in rings A (where the largest changes in bond order take place) of the special-pair BChls (P, temporarily named 'P_L' and 'P_M') overlap. In the overlap region, indicated by a black circle, separation is as little as 3.43 Å (i.e., van der Waals contact) thus facilitating charge separation.

Electron Transfer from one of the Special-Pair BChls (P_M) to the Accessory BChl (B_L) and then to the BPhe (H_L). Figure 5b shows that the C_b–C_b bond in ring A of P_M is close to that in ring C of B_L (the smallest distance, 5.63 Å), whereas Fig. 5c shows that the C_b–C_b bond in ring A of B_L is close to that in ring A of H_L (the smallest distance, 5.16 Å). The pigment arrangements described above must enhance the series of electron-transfer reactions in the order, $P_M \rightarrow B_L \rightarrow H_L$, where the regions of the largest changes in bond order of both the donor and the acceptor are used.

Triplet-energy Transfer from one of the Special-pair BChls (P_M) to the Accessory BChl on the M Branch (B_M), and then to the Car. Figure 5d shows that a C_a–N bond in ring C of P_M is close to a $C_{a'}$–$C_{b'}$ bond in ring B of B_M (the smallest distance, 5.42 Å), whereas Fig. 5e shows that a C_a–N bond of B_M is in close contact with the C13=C14 bond of Car (the smallest distance, 4.49 Å). The arrangements must facilitate the triplet energy-transfer reactions in the order $P_M \rightarrow B_M \rightarrow$ Car; here, the region of the second-largest change in bond order of the donor and that of the largest change in bond order of the acceptor are used. No efficient triplet-energy transfer is expected between the B_M and H_M molecules (Fig. 5f).

It is to be noted that each pair of pigments on the L and M branches exhibit approximate C_2 symmetry. In general, the arrangement of the BChl and BPhe molecules on the L branch enabling the extremely fast charge-separation and electron-transfer reactions seems to be of first priority. The arrangement of BChl molecules on the M branch to facilitate the much slower triplet energy-transfer reaction may be less important. It cannot be over-emphasized that the P_L, P_M, B_L and H_L molecules are perfectly arranged to achieve the overlap of C_b–C_b bonds thereby promoting the most important charge-separation and electron-transfer reactions in the RC.

III. Generation of the T_1 State and Subsequent Transformation into the D_0 State upon Photo-Excitation of in vitro and in vivo Bacteriochlorophyll *a* Aggregates

A. Bachteriochlorophyll a Aggregates in Solution

The generation of the D_0 state by photo-excitation of BChl *a* aggregates was first identified in methylene chloride and carbon tetrachloride solutions and the ring-breathing Raman lines appeared at 1597 and 1599 cm^{-1}, respectively (Nishizawa et al., 1994a), which is in the region of the 5-coordinated radical cation (1595–1599 cm^{-1}); see Table 1 or Table S1.

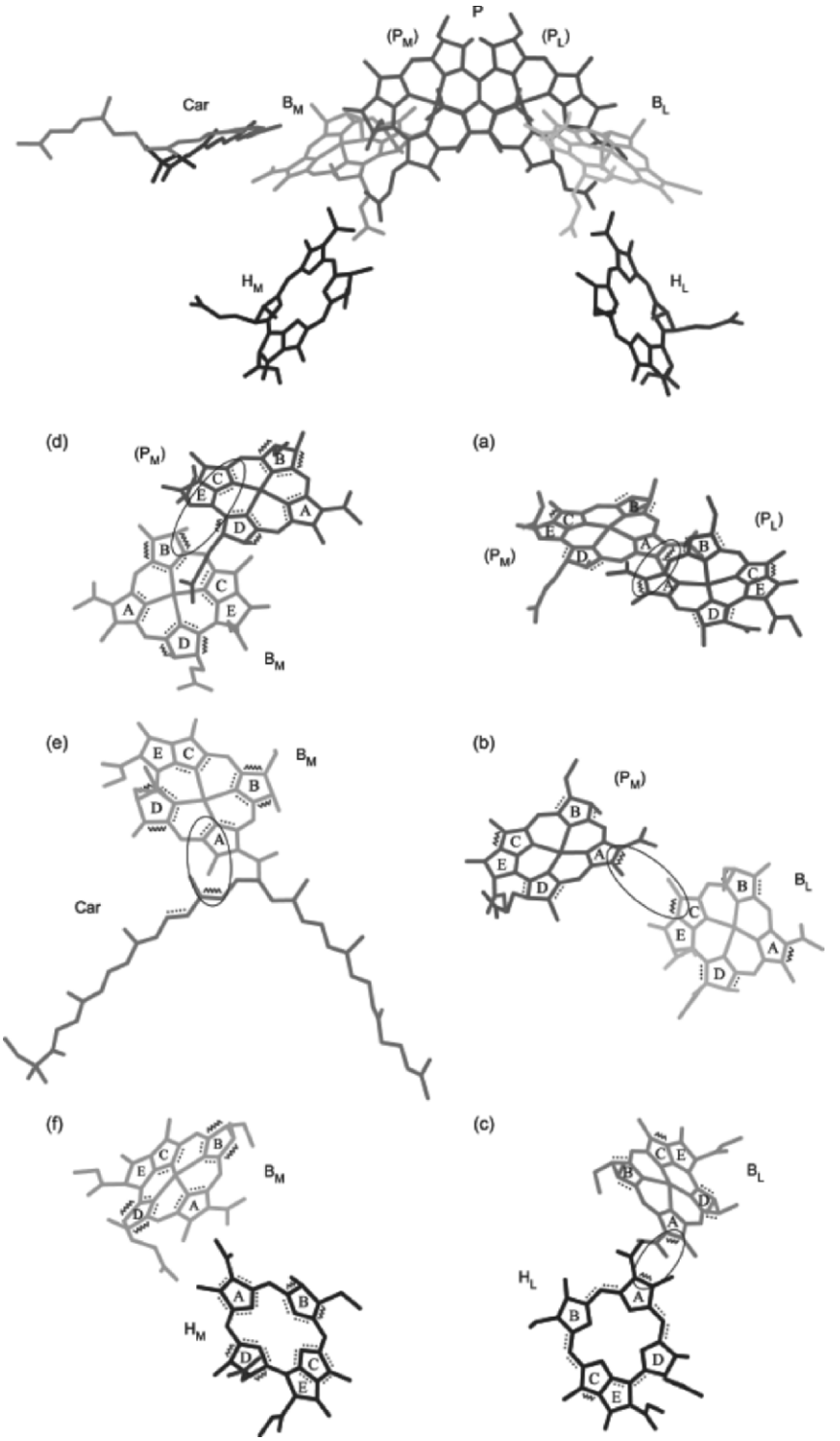

Fig. 5. Spatial arrangement of the special pair BChls (P, tentatively named 'P_L' and 'P_M'), the accessory BChls (B_L and B_M), the BPhes (H_L and H_M) and the Car molecules in the RC from *Rba. sphaeroides* strain AM260W (R. J. Cogdell, personal communication). The regions where the largest and the second-largest changes in bond order take place (where the HOMO and/or the LUMO are/is expected to be most or second-most localized) are indicated by wavy and dotted lines, in each pigment molecule (see Fig. 4); further, overlap of those regions is indicated by a black circle for each pigment pair. See also Color Plate 2.

Actually, the Raman spectrum of the transient species in methylene chloride agrees, within the limit of experimental error, with the stationary-state Raman spectrum of the radical cation (Fig. S2-g). Since both methylene chloride and carbon tetrachloride are chlorine-containing solvents forming BChl *a* aggregates, the electron ejected from BChl *a* to form BChl $a^{+\bullet}$ (the radical cation) is most probably transferred to the entire aggregate to form $BChl_n^{-\bullet}$ and, subsequently, to the chlorine atom in the solvent to form $Cl^{-\bullet}$.

Definitive evidence for the generation of the radical-cation (D_0) state by photo-excitation was obtained by time-resolved absorption spectroscopy of BChl *a* aggregates in carbon tetrachloride solution (Nishizawa et al., 1994b): Figure 6a shows the transient absorption spectrum of BChl *a* in pyridine (a 6-coordinating solvent): The absorption spectrum is typical of the T_1 state (Connolly et al., 1973; Nishizawa et al., 1994b). On the other hand, Fig. 6b shows the transient absorption spectrum of BChl *a* in carbon tetrachloride, which is consistent with the stationary-state absorption spectrum of BChl *a* radical cation that was electrochemically generated by one-electron oxidation (Misono et al., 1996). Thus, the radical cation (D_0 state) can be generated within 200 ns after excitation in carbon tetrachloride forming a higher aggregate.

Transformation from the T_1 state to the D_0 state was traced by time-resolved absorption spectroscopy of BChl *a* in methylene chloride solution (Nishizawa et al., 1994b); Figs. 6c, d and e show time-resolved absorption spectra recorded at 200 ns, 1 μs and 100 μs after excitation, respectively. Spectrum (c) exhibits the contribution of the T_1 state (401 nm) as the major component and that of the D_0 state as a minor component (a shoulder ~420 nm); spectrum (d) exhibits comparable intensity contributions by both states; and spectrum (e) exhibits only the contribution of the D_0 state. Spectrum (e) is almost identical to the stationary-state absorption spectrum of the D_0 state electrochemically generated in this particular solvent (see Fig. 5a of Misono et al., 1996). When spectrum (e) is subtracted from spectrum (c), spectrum (f) emerges as a pure T_1-state spectrum thus identifying

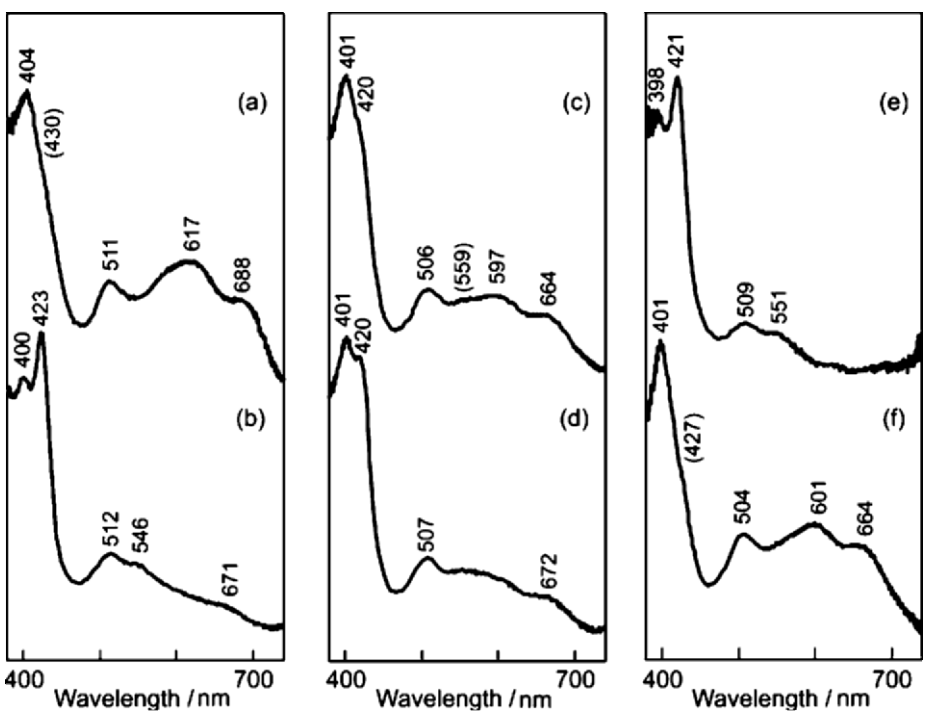

Fig. 6. (a) The transient T_1-state spectrum of BChl *a* monomer in pyridine, and (b) the transient D_0-state spectrum of BChl *a* aggregates in carbon tetrachloride, both at 200 ns after excitation. Time-resolved absorption spectra showing transformation from the T_1 to the D_0 state for BChl *a* aggregates in methylene chloride at (c) 200 ns, (d) 1 μs and (e) 100 μs after excitation. The difference spectrum (f) of (c) minus (e) exhibits the T_1-state spectrum, whereas spectrum (e) shows a pure D_0-state spectrum. Each sample solution was excited by the use of the 355nm, 12 ns pulses.

Table 2. The g-values, the linewidths and the lifetimes of the EPR signals from radical cation generated by photo-excitation of BChl *a* aggregates in carbon tetrachloride and in the carotenoid-less LH1, LH2 and RC complexes (at 110 K)

BChl *a* aggregates in	g-value	ΔH_{pp} [a] (gauss)	line shape	lifetime (ms)
CCl_4 solution	2.0026 ± 0.0002	12.3 ± 0.5	G [b]	5 ± 1
LH1	2.0026 ± 0.0002	9.3 ± 0.2	G	27 ± 3
LH2	2.0026 ± 0.0002	9.3 ± 0.2	G	27 ± 3
RC	2.0026 ± 0.0002	10.3 ± 0.2	G	25 ± 3

[a] ΔH_{pp} indicates peak-to-peak first-derivative linewidth. [b] G indicates the Gaussian line shape.

the T_1 state as the precursor of the D_0 state in methylene chloride forming a lower aggregate.

The generation of radical cation (the D_0 state) by photo-excitation of the BChl *a* aggregate in carbon tetrachloride was established by EPR spectroscopy (Limantara et al., 1998). Table 2 shows the g-value, the linewidth, the line shape and the lifetime of this radical-cation signal. (Figure S6 shows a raw EPR spectrum of the D_0 state generated by photo-excitation of BChl *a* aggregates in carbon tetrachloride.)

B. Carotenoid-less Antenna Complexes

Limantara et al. (1998) discovered, by picosecond and nanosecond transient Raman spectroscopy, the generation of the T_1 state and its subsequent transformation into the D_0 state in the carotenoid-less LH1 and LH2 antenna complexes from *Rba. sphaeroides* R26 and R26.1. Here, the frequencies of the ν_r'' and ν_r^+ modes described in Sec. I played a key role. In transient Raman spectroscopy using ~50 ps pulses, the LH1 and LH2 complexes exhibited the ring-breathing Raman lines at 1590 and 1589 cm^{-1}, indicating that T_1 BChl *a* in the 5-coordinated state (the ν_r'' frequency region, 1585–1591 cm^{-1}) was generated during the pulse duration of ~50 ps (Table 1). On the other hand, the RC complex exhibited the ring-breathing Raman line at 1598 cm^{-1}, indicating, instead, that D_0 BChl *a* in the 5-coordinated state (the ν_r^+ frequency region, 1595–1599 cm^{-1}) is generated within 2.8 ps (Martin et al., 1986). (Figure S7 compares the S_0 Raman spectra (1) and transient Raman spectra obtained by the use of the ~50 ps pulses and ~12 ns (2 and 3, respectively) among the (a) LH1, (b) LH2 and (c) RC complexes from *Rba. sphaeroides* R26 and R26.1.)

In transient Raman spectroscopy using 12 ns pulses, both the LH1 and LH2 complexes exhibited transient ring-breathing Raman lines at 1596 cm^{-1} indicating that the T_1 state had already transformed into the D_0, 5-coordinated state within that particular pulse duration; see the ν_r'' and ν_r^+ frequency regions shown above. Again, the RC complex exhibited the ring-breathing Raman line at 1599 cm^{-1}, indicating that the D_0 state still remains. Thus, the generation of the D_0 state via the T_1 state by photo-excitation of the ring-shaped BChl *a* aggregates in the carotenoid-less antenna complexes was identified by transient Raman spectroscopy using the picosecond and the nanosecond pulses. In all the S_0, T_1 and D_0 states, the ring-breathing frequencies show that the BChl *a* molecules in the LH1, LH2 and RC complexes are in the 5-coordinated state.

The generation of the radical cation (D_0 state) by photo-excitation of the carotenoid-less LH1 and LH2 complexes was confirmed by EPR spectroscopy. Table 2 shows the g-values, the linewidths, the line shapes and the lifetimes of the radical cation signals generated in the LH1, LH2 and RC complexes. (Figure S6 shows the raw EPR signals of the carotenoid-less LH1, LH2 and RC complexes.) Comparison of the linewidths shows that the extent of electron delocalization is in the following order: LH1 and LH2 antenna complexes < RC < in vitro aggregates in carbon tetrachloride solution.

Most importantly, the precursor of the radical cation, i.e., T_1 BChl *a*, is quenched by Car, all-*trans*-spheroidene, in the LH1 and LH2 complexes from the wild type *Rba. sphaeroides*, preventing the oxidative degradation of the BChl *a* molecules (Limantara et al., 1998).

Acknowledgments

The authors thank Prof. Hugo Scheer, Prof. Hiroyoshi Nagae and Dr. Leszek Fiedor for reading the manuscript. This work has been supported by a grant from NEDO (New Energy and Industrial Technol-

ogy Development Organization, 'International Joint Research Grant'), and a grant from the Ministry and Education, Culture, Sports, Science and Technology for an Open Research Center Project, 'The Research Center of Photo-Energy Conversion.'

References

Callahan PM and Cotton TM (1987) Assignment of bacteriochlorophyll *a* ligation state from absorption and resonance Raman spectra. J Am Chem Soc 109: 7001–7007

Connolly JS, Gorman DS and Seely GR (1973) Laser flash photolysis studies of chlorin and porphyrin systems. I. Energetics of the triplet state of bacteriochlorophyll. Ann NY Acad Sci 206: 649–669

Donohoe RJ, Frank HA and Bocian DF (1988) Resonance Raman spectra and normal mode descriptions of a bacteriochlorophyll *a* model complex. Photochem Photobiol 48: 531–537

Gutmann V (1978) The Donor-Acceptor Approach to Molecular Interactions. Plenum Press, New York

Hu S, Mukherjee A and Spiro TG (1993) Synthesis, vibrational spectra, and normal mode analysis of nickel(II) 1,5-dihydroxy-1,5-dimethyloctaethylbacteriochlorin: A model for bacteriochlorophylls. J Am Chem Soc 115: 12366–12377

Kamlet MJ and Taft RW (1979) Linear solvation energy relationships. Part 1. Solvent polarity-polarizability effects on infrared spectra. J Chem Soc Perkin Trans 2: 337–341

Kamlet MJ, Abboud JL and Taft RW (1977) The solvatochromic comparison method. 6. The π* scale of solvent polarities. J Am Chem Soc 99: 6027–6038

Kamlet MJ, Abboud J-L M, Abraham MH and Taft RW (1983) Linear solvation energy relationships. 23. A comprehensive collection of the solvatochromic parameters, π*, α, and β, and some methods for simplifying the generalized solvatochromic equation. J Org Chem 48: 2877–2887

Koyama Y and Limantara L (1998) Effects of singlet and triplet excitation, oxidation and axial coordination on the bond orders in the macrocycle of bacteriochlorophyll *a* as revealed by resonance Raman spectroscopy. Spectrochim Acta Part A 54: 1127–1139

Limantara L, Fujii R, Zhang J-P, Kakuno T, Hara H, Kawamori A, Yagura T, Cogdell RJ and Koyama Y (1998) Generation of triplet and cation-radical bacteriochlorophyll *a* in carotenoidless LH1 and LH2 antenna complexes from *Rhodobacter sphaeroides*. Biochemistry 37: 17469–17486

Lutz M (1984) Resonance Raman studies in photosynthesis. In: Clark RJH and Hester RE (eds) Advances in Infrared and Raman Spectroscopy, Vol 11, pp 211–300. John Wiley & Sons, Chichester

Martin J-L, Breton J, Hoff AJ, Migus A and Antonetti A (1986) Femtosecond spectroscopy of electron transfer in the reaction center of the photosynthetic bacterium *Rhodopseudomonas sphaeroides* R-26: Direct electron transfer from the dimeric bacteriochlorophyll primary donor to the bacteriopheophytin acceptor with a time constant of 2.8 ± 0.2 psec. Proc Natl Acad Sci USA 83: 957–961

Misono Y, Limantara L, Koyama Y and Itoh K (1996) Solvent effects on the resonance Raman and electronic absorption spectra of bacteriochlorophyll *a* cation radical. J Phys Chem 100: 2422–2429

Mukai-Kuroda Y, Fujii R, Ko-chi N, Sashima T, Koyama Y, Abe M, Gebhard R, van der Hoef I and Lugtenburg J (2002) Changes in molecular structure upon triplet excitation of all-*trans*-spheroidene in *n*-hexane solution and 15-*cis*-spheroidene bound to the photo-reaction center from *Rhodobacter sphaeroides* as revealed by resonance-Raman spectroscopy and normal-coordinate analysis. J Phys Chem A 106: 3566–3579

Nishizawa E, Limantara L, Nanjou N, Nagae H, Kakuno T and Koyama Y (1994a) Solvent effects on triplet-state bacteriochlorophyll *a* as detected by transient Raman spectroscopy and the environment of bacteriochlorophyll *a* in the light-harvesting complex of *Rhodobacter sphaeroides* R26. Photochem Photobiol 59: 229–236

Nishizawa E, Nagae H and Koyama Y (1994b) Transient absorption spectroscopy of bacteriochlorophyll *a*: Cation radical generated in solvents forming aggregates and T_1 species generated in solvents forming penta- and hexacoordinated monomers with and without hydrogen bonding. J Phys Chem 98: 12086–12090

Sashima T, Limantara L and Koyama Y (2000) Changes in the carbon-carbon and carbon-nitrogen stretching force constants in the macrocycles of bacteriochlorophyll *a* and bacteriopheophytin *a* upon triplet and singlet excitation: Resonance-Raman spectroscopy and normal-coordinate analysis of the unlabeled and totally ^{15}N-, ^{13}C-, and ^{2}H-labeled species. J Phys Chem B 104: 8308–8320